THE JOURNAL OF PHYSICAL CHEMISTRY Letters

Letter

Cite This: J. Phys. Chem. Lett. 2019, 10, 2295−2299

pubs.acs.org/JPCL

Correlated Multimodal Approach Reveals Key Details of Nerve-Agent Decomposition by Single-Site Zr-Based Polyoxometalates

Yiyao Tian,[†] Anna M. Plonka,[†] Amani M. Ebrahim,[†] Robert M. Palomino,[‡] Sanjaya D. Senanayake,[‡] Alex Balboa,[§] Wesley O. Gordon,[§] Diego Troya,[∥] Djamaladdin G. Musaev,[⊥,#] John R. Morris,[∥] Mark B. Mitchell,[▽] Daniel L. Collins-Wildman,[#] Craig L. Hill,[#] and Anatoly I. Frenkel*[,†,‡]

[†]Department of Materials Science and Chemical Engineering, Stony Brook University, Stony Brook, New York 11794, United States

[‡]Chemistry Division, Brookhaven National Laboratory, Upton, New York 11973, United States

[§]U.S. Army Edgewood Chemical Biological Center, Aberdeen Proving Ground, Maryland 21010, United States

[∥]Department of Chemistry, Virginia Tech, Blacksburg, Virginia 24061, United States

[⊥]Cherry L. Emerson Center for Scientific Computation, Emory University, Atlanta, Georgia 30322, United States

[#]Department of Chemistry, Emory University, Atlanta, Georgia 30322, United States

[▽]Department of Chemistry, Kennesaw State University, Kennesaw, Georgia 30144, United States

Supporting Information

ABSTRACT: Development of technologies for protection against chemical warfare agents (CWAs) is critically important. Recently, polyoxometalates have attracted attention as potential catalysts for nerve-agent decomposition. Improvement of their effectiveness in real operating conditions requires an atomic-level understanding of CWA decomposition at the gas−solid interface. We investigated decomposition of the nerve agent Sarin and its simulant, dimethyl chlorophosphate (DMCP), by zirconium polytungstate. Using a multimodal approach, we showed that upon DMCP and Sarin exposure the dimeric tungstate undergoes monomerization, making coordinatively unsaturated Zr(IV) centers available, which activate nucleophilic hydrolysis. Further, DMCP is shown to be a good model system of reduced toxicity for studies of CWA deactivation at the gas−solid interface.

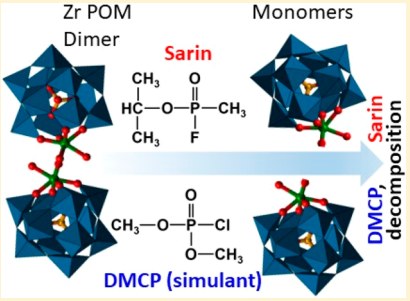

Chemical warfare agents (CWAs), in particular, organophosphorus (OP) nerve agents such as VX, Sarin (GB), and Soman, continue to present a threat to both military and civilian populations,[1−3] even though decontamination strategies have been investigated for many decades.[2,4,5] Previous approaches have included oxidation, detoxification, and degradation of OPs via biochemical approaches.[6] Recently, a new generation of sorptive or catalytically active materials, including metal oxide/hydroxide-based formulations,[7,8] metal−organic frameworks (MOFs),[9−13] and polyoxometalates (POMs),[5,14−19] has been reported. POMs contain inorganic metal−oxygen clusters with highly tunable properties[20] and are currently being actively considered as reactive sorbents for the decontamination of CWAs. Their stability, combined with their extensively alterable molecular properties, make them widely attractive in materials science,[21] medicine,[22] and catalysis.[23,24] In addition to niobium-based POMs,[14−16,25] which exhibit limited catalytic OP decontamination, the zirconium-substituted POM, $(Et_2NH_2)_8[\{\alpha\text{-}PW_{11}O_{39}Zr(\mu\text{-}OH)(H_2O)\}_2]\cdot 7H_2O$ (Zr-POM), was recently shown to catalyze decomposition of the nerve-agent simulant, methyl paraoxon, in a homogeneous buffered solution.[26] This Zr-POM, however, has yet to be studied as a heterogeneous catalyst at the gas−solid interface. Therefore, a fundamental study on the interactions of solid-state Zr-POMs with gaseous OPs is needed to provide insight into application of this material for nerve-agent decontamination, specifically when OPs are delivered in the vapor phase.

In this work, we utilized a multimodal approach for investigating a reaction of gaseous dimethyl chlorophosphate, DMCP (a GB simulant) with Zr-POM. The purpose was to detect the changes in both the Zr-POM and agent/simulant upon exposure and to evaluate the quality of DMCP as a less toxic compound for simulating the heterogeneous chemistry of GB.

To probe the GB and DMCP (Figure S1) adsorption and reaction on the solid Zr-POM, we performed XPS measurements. The spectra show signatures of POM-bound decomposition products of GB and DMCP and reveal changes to the electronic structure of Zr centers. The Zr 3d XPS peak positions of the pristine Zr-POM prior to DMCP exposure agree with those in ZrO_2. The binding energies of Zr $3d_{3/2}$ and

Received: April 8, 2019
Accepted: April 19, 2019
Published: April 19, 2019

DOI: 10.1021/acs.jpclett.9b01002
J. Phys. Chem. Lett. 2019, 10, 2295−2299

Zr $3d_{5/2}$ electrons are 185.0 and 182.7 eV, respectively (Figure 1a), consistent with previous reports.[27] The Zr 3d peaks

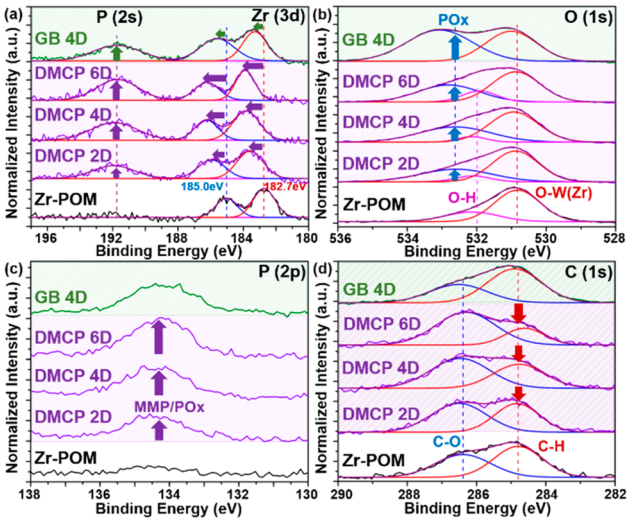

Figure 1. XPS spectra of Zr-POM exposed to GB and DMCP with fitted Gaussian components: (a) P(2s) and Zr(3d), (b) O(1s), (c) P(2p), and (d) C(1s). "D" in the inset text means "days" for DMCP or GB exposure times on Zr-POM. MMP is methyl methylphosphate (a decomposition product of DMCP).

increasingly shift to higher binding energy with DMCP exposure time, indicating strong interaction between Zr and electron-withdrawing ligands, consistent with the formation of bound phosphate species (vide infra).[27] A similar shift is observed in the Zr 3d XPS signal obtained after exposure of Zr-POM to GB (Figure 1a). The O(1s) spectrum of pristine Zr-POM (Figure 1b) shows a two-peak feature, assigned to surface-bound −OH and O−W(Zr) bonds. The O−W(Zr) peak remains unchanged upon DMCP exposure, but the −OH feature exhibits some variation as exposure proceeds, suggesting its involvement in the adsorption/reaction. A new feature at 533 eV appears and grows after DMCP exposure, indicating the bound phosphate species. The surface-bound product species are also seen in the peaks assigned to P═O in the P(2s) and P(2p) regions in the spectra of DMCP-treated samples (Figure 1a,c). The increase in the intensity of phosphate species with exposure identifies DMCP adsorption to the surface and, together with the observed decrease of C−H species and increase of C−O species (Figure 1d), confirms reaction and decomposition of DMCP on the Zr-POM. Similar effects were observed when Zr-POM was exposed to GB, namely, the appearance of the P(2s) and P(2p) peaks (Figure 1a,c) and the POx peak in the O(1s) region (Figure 1b). Zr-POM is therefore active for decomposition of both DMCP and GB. The absence of Cl(1s) and presence of F(1s) signals (Figure S2a,b) can be attributed to the different binding strengths of the DMCP and GB decomposition products, respectively.

To augment the XPS results and gather additional information about the DMCP and GB decomposition, we performed diffuse reflectance infrared Fourier transform spectroscopy (DRIFTS) experiments. In the in situ difference DRIFT spectra during DMCP exposure of Zr-POM (Figure S3), the peak at ∼1230 cm^{-1} is due to hydrogen bonding of P═O, which is associated with physisorbed DMCP.[28] Using calculated spectra of DMCP (Figure S4), the overlapping bands between 1200 and 1100 cm^{-1} can be assigned to symmetric and asymmetric O−P−O stretches, mixed in with modes belonging to chemically reacted species of DMCP.[27] The peak at ∼1025 cm^{-1} is a merged contribution from the symmetric and asymmetric C−O−P stretches. These bands provide evidence of decomposition of DMCP when absorbed on Zr-POM, consistent with our XPS measurements. The overlapping bands were also observed in the spectra of GB on Zr-POM (Figure S5), indicating similar products for decomposition of GB.

As a result of the Zr-POM and DMCP (and GB) interaction, significant changes occur not only to adsorbed molecules but also to the Zr-POM (Figure 2a). In the O−H stretching region

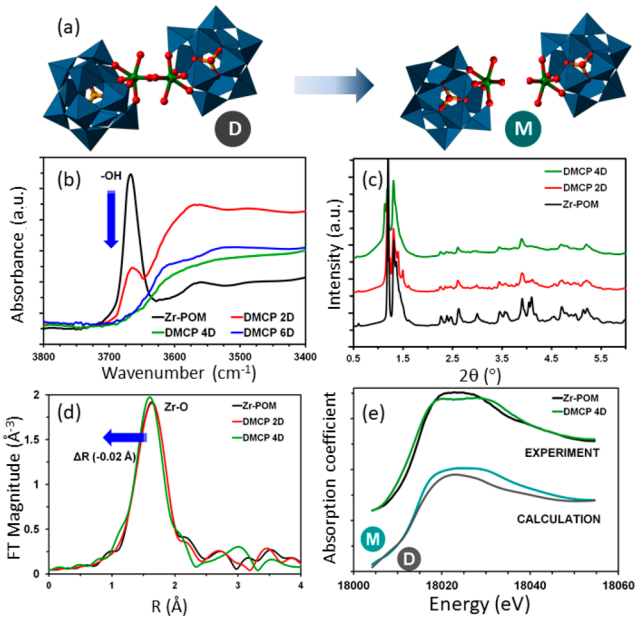

Figure 2. (a) Dissociation of Zr-POM dimers (**D**) to monomers (**M**) after the exposure of Zr-POM to DMCP; (b) DRIFTS spectra of the bridging O−H region demonstrate a decrease in the number of O−H species in the Zr-POM dimer; (c) X-ray powder diffraction (PXRD) pattern suggesting increased disorder of the Zr-POM upon CWA exposure; (d) Zr K-edge EXAFS spectra in Zr-POM shift to lower Zr−O distances; (e) the evolutions of experimental (before and after DMCP exposure) and calculated (dimers vs monomers) Zr K-edge XANES spectra are similar.

for the pristine Zr-POM, a narrow band with a peak at 3670 cm^{-1} and a broader band between 3620 and 3520 cm^{-1} are present in the DRIFTS spectrum. On the basis of the Zr-POM dimer structure (Figure S6), the 3670 cm^{-1} band is assigned to the dimer bridging O−H species, consistent with the vibrational frequency of bridging O−H species in $Zr(OH)_4$ and in ZrO_2 (Figure S7). To support this assignment, we collected DRIFTS spectra of aqua-free Zr-POM (it has a similar structure as the Zr-POM dimer and also includes bridging O−H species but without water coordinated to Zr atoms[29]) during thermal treatment (Figure S8). The 3657 cm^{-1} peak of the aqua-free Zr-POM persists, suggesting that the 3670 cm^{-1} absorption in the Zr-POM dimer originates in the bridging O−H species. The feature between 3620 and 3520 cm^{-1} is assigned to molecular water with hydrogen-bonding interactions in the dimer, as supported by the decrease in the band intensity during thermal treatment (Figure S9). After 2 days of exposure to DMCP (Figure 2b),

DOI: 10.1021/acs.jpclett.9b01002
J. Phys. Chem. Lett. 2019, 10, 2295−2299

there is a significant loss of intensity in the sharp O−H feature and growth of the broad O−H feature at lower frequency, which together result from hydrogen bonding between DMCP and the bridging O−H species.[30,31] As the exposure continues, the intensity of the sharp O−H absorption virtually disappears, while the intensity of the broad O−H feature nearly returns to its value prior to exposure. These results suggest that the DMCP interaction results in complete loss of the bridging O−H species.

The same trend in the intensity of the bridging O−H feature is observed when Zr-POM is exposed to GB (Figure S5). However, the reaction with GB also leads to a significant loss of the aqua ligands, which does not occur in the reaction with DMCP, indicating that the GB reaction consumes water through hydrolysis.

Synchrotron XRD (Figure 2c) and Zr K-edge XAFS (Figure 2d,e) were employed to probe the structural changes of the Zr-POM after exposure to DMCP. EXAFS (Figure S10) revealed the same Zr−O bond length (2.16 Å) in pristine Zr-POM as that in the theoretical dimer structure (Table S1), indicating that dimers dominate the as-synthesized sample. This conclusion was corroborated by PXRD measurements (Figure S11), which also show that the Zr-POM lattice became disordered with exposure to DMCP (Table S2). A decrease of the Zr−O bond length from 2.16 to 2.14 Å was observed by EXAFS analysis (Figure 2d) in Zr-POM exposed to DMCP after 4 days, which was accompanied by strong changes in the XANES spectra (Figure 2e). The best agreement with the observations was obtained when the theoretical XANES spectra of the dimer and monomer were compared. Dissociation from dimers to monomers explains also the EXAFS data because the average Zr−O distance in the calculated monomer structure (2.09 Å) is shorter than that in the dimer (2.16 Å) (Figure S12). Therefore, EXAFS results obtained after DMCP exposure correspond to a mixture of dimers and monomers, effectively lowering the average Zr−O distance compared to that in pure dimer.

Correlating Raman spectroscopic results with those discussed above was critical for deciphering the overall mechanism. Specifically, the appearance of a band at around 2862 cm^{-1} following exposure, attributed to the symmetric stretch of CH_3, is due to adsorbed DMCP (Figure S13d). Furthermore, broadening and blue shifting of the Zr-POM band at around 997 cm^{-1}, attributed to the $W{-}O_{terminal}$ stretch, is observed after DMCP exposure[32] (Figure S13c). The shoulder at 985 cm^{-1} disappears with gas exposure. Some bands in the 300−500 cm^{-1} range, where bridging Zr−O−Zr normal modes contribute, broaden or disappear after DMCP exposure (Figure S13b). These changes are weak or absent after water exposure (Figure S14), implying that DMCP affects the Zr-POM structure to a larger extent than just water. These spectral changes differ from those following exposure to HCl (Figure S15), suggesting that DMCP (as opposed to its decomposition product, HCl) causes changes to the framework.

We turned to computation to elucidate the impact of DMCP and GB gases on the observed monomerization of the dimer (**D**) upon exposure (Figure S6b) and to reveal the role of the monomers (**M**) in the decomposition of DMCP and GB. We calculated the energetics of monomerization of **D**, i.e., **D** → 2**M** rearrangement (Figure S6a), in the absence of warfare gases and found that this process entails $\Delta H/\Delta G$ = 38.5/8.8 kJ/mol (Figure S16). The coordination of DMCP and GB molecules to dimer **D** results in the formation of the **D-CWA** adduct (where CWA = DMCP or GB), and the calculated **D-CWA** interaction energy is 61.5/8.0 and 58.2/14.1 kJ/mol for DMCP and GB, respectively. In the results of this **D-CWA** perturbative interaction, the enthalpy required for monomerization of the dimer decreases (from 38.5 kJ/mol) to 12.6 and 14.2 kJ/mol, while at the Gibbs free energy level, the dimer species becomes by 43.5 and 41.4 kJ/mol less stable than for the two separate monomers (Figure S16).

Because DMCP interacts with the dimer slightly stronger than GB, one would expect the monomerization of **D** to be easier while interacting with DMCP than GB, as confirmed by Figure S16. Indeed, while the **D-CWA** interaction enthalpy is 3.3 kJ/mol larger for DMCP than that for GB, the monomerization enthalpy is only 1.7 kJ/mol smaller for GB than that for DMCP. Analyses of the geometries of the related complexes show that this could be the result of asymmetric coordination of GB to **D** compared with DMCP. As shown in Figure S17, in their respective **D-CWA** adducts, DMCP interacts with both POM fragments of **D**, but GB interacts with only one of them. This asymmetric coordination/interaction of GB with dimer **D** induces a stronger disturbance to one of the POM fragments and facilitates its easier dissociation.

Electronic structure calculations (Figure 3) revealed that the destruction of DMCP upon reaction with the Zr-POM

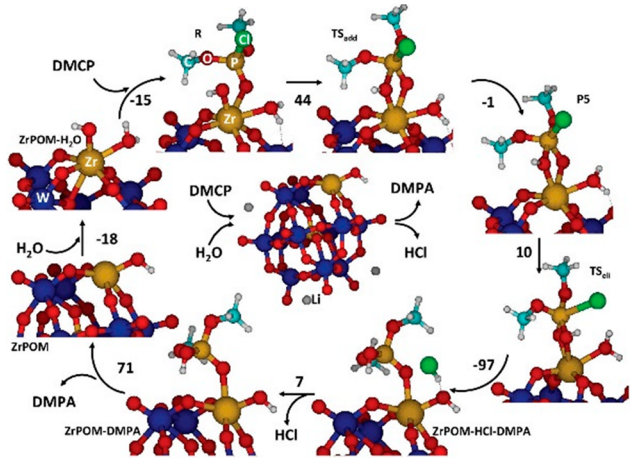

Figure 3. Hydrolysis reaction mechanism for DMCP on the Zr-POM monomers, showing DMCP binding, OH/HCl addition/elimination, product desorption, and catalyst regeneration. Numbers correspond to 298 K Gibbs energies (kJ/mol) calculated at the M06-L/[6-31G**+Lanl2dz] level.

monomers occurs via a general base hydrolysis mechanism.[18,33] Monomerization results in an undercoordinated Zr(IV) Lewis acid site available to bind DMCP, producing the hydrolysis reaction complex (R). Reaction is initiated by the nucleophilic addition of a Zr hydroxo ligand to the bound DMCP. This addition process occurs through a moderate barrier of 44 kJ/mol (TS_{add}) and leads to a shallow pentacoordinated phosphorus intermediate (P5). Reaction continues through Cl elimination with a proton of the aqua ligand of Zr (TS_{eli}) to form HCl and the dimethyl ester of phosphoric acid (DMPA). The elimination process is notably exergonic and leads to bound HCl and DMPA. Desorption of HCl is facile, leaving DMPA bound on the Zr center of the Zr-POM. A noteworthy aspect of this phosphate product is that it is bound by only one

DOI: 10.1021/acs.jpclett.9b01002
J. Phys. Chem. Lett. 2019, 10, 2295−2299

coordinate covalent bond to the Zr center. Recent work with Zr-MOFs has suggested the possibility of strong bidentate binding of the OP hydrolysis products on the MOFs, which cannot be thermally removed without decomposing the MOF itself.[34,35] The bidentate binding in MOFs is elicited by the presence of adjacent Zr sites, which are not present in the single-site Zr-POM monomer of this work. Consequently, the desorption energy of the phosphate product from Zr-POM requires less than half of the energy as that from the Zr-MOFs, which elevates the promise of catalyst regeneration in the single-site molecular solid. The catalytic cycle is completed by DMPA product desorption and binding of ambient water.

In summary, our multimodal approach allowed us to investigate active sites and their roles in the process of OP compound decomposition by an effective nerve-agent hydrolysis solid at the gas−solid interface, i.e., in realistic battlefield conditions. We have shown that upon DMCP and Sarin exposure the Zr-POM dimer transforms to the Zr-POM monomer with a coordinatively unsaturated Zr(IV) center. The latter is a key species in a catalytic cycle that binds nerve agents and decomposes them via a nucleophilic (general base) hydrolysis mechanism. The isolation of one Zr atom in the Zr-POM of this work ameliorates product inhibition because the hydrolysis product does not bind to the catalyst very strongly. We found a strong similarity in the surface chemistry of DMCP and GB by direct comparison of several spectroscopic probes. As such, DMCP is proposed as a model system in the development of catalysts for CWA deactivation under relevant battlefield conditions.

■ ASSOCIATED CONTENT

Supporting Information

The Supporting Information is available free of charge on the ACS Publications website at DOI: 10.1021/acs.jpclett.9b01002.

Experimental details on materials, materials characterization, X-ray photoelectron spectroscopy, X-ray absorption fine structure spectroscopy, X-ray diffraction, diffuse reflectance infrared Fourier transform spectroscopy, Raman spectroscopy, and supporting figures (PDF)

■ AUTHOR INFORMATION

Corresponding Author

*E-mail: anatoly.frenkel@stonybrook.edu.

ORCID

Yiyao Tian: 0000-0002-8148-9375
Anna M. Plonka: 0000-0003-2606-0477
Robert M. Palomino: 0000-0003-4476-3512
Sanjaya D. Senanayake: 0000-0003-3991-4232
Diego Troya: 0000-0003-4971-4998
Djamaladdin G. Musaev: 0000-0003-1160-6131
John R. Morris: 0000-0001-9140-5211
Craig L. Hill: 0000-0002-5506-9588
Anatoly I. Frenkel: 0000-0002-5451-1207

Notes

The authors declare no competing financial interest.

■ ACKNOWLEDGMENTS

This work is supported by the U.S. Army Research Laboratory and the U.S. Army Research Office under Grant Number W911NF-15-2-0107. We thank the Defense Threat Reduction Agency for support under Program BB11PHM156. R.M.P. was partially funded by NSF Grant 1311318. Reaction tests at the Brookhaven National Laboratory (BNL) Chemistry Division were made possible due to the Laboratory Directed Research and Development Program through LDRD 18-047 fund to A.I.F. XPS measurements were conducted at the BNL Chemistry Division, supported by the U.S. Department of Energy, Office of Science, Basic Energy Sciences, Chemical Science, Geosciences and Biosciences Division under Contract No. DE-SC0012704. S.D.S. is supported by a U.S. Department of Energy, Office of Science, Basic Energy Sciences Early Career Award. Use of the SSRL and NSLS-II was supported by the DOE under Contracts DE-AC02-76SF00515 and DE-SC0012704, respectively. We acknowledge Advanced Research Computing at Virginia Tech and the Cherry L. Emerson Center for Scientific Computation at Emory University for providing computational resources and technical support.

■ REFERENCES

(1) Szinicz, L. History of Chemical and Biological Warfare Agents. *Toxicology* **2005**, *214*, 167−181.
(2) Yang, Y.-C.; Baker, J. A.; Ward, J. R. Decontamination of Chemical Warfare Agents. *Chem. Rev.* **1992**, *92*, 1729−1743.
(3) Dixon, M.; Needham, D. M. Biomedical Research on Chemical Warfare Agents. *Nature* **1946**, *158*, 432−438.
(4) Stone, H.; See, D.; Smiley, A.; Ellingson, A.; Schimmoeller, J.; Oudejans, L. Surface Decontamination for Blister Agents Lewisite, Sulfur Mustard and Agent Yellow, a Lewisite and Sulfur Mustard Mixture. *J. Hazard. Mater.* **2016**, *314*, 59−66.
(5) Kim, K.; Tsay, O. G.; Atwood, D. A.; Churchill, D. G. Destruction and Detection of Chemical Warfare Agents. *Chem. Rev.* **2011**, *111*, 5345−5403.
(6) Raber, E.; McGuire, R. Oxidative Decontamination of Chemical and Biological Warfare Agents using L-Gel. *J. Hazard. Mater.* **2002**, *B93*, 339−352.
(7) Wagner, G. W.; Procell, L. R.; O'Connor, R. J.; Munavalli, S.; Carnes, C. L.; Kapoor, P. N.; Klabunde, K. J. Reactions of VX, GB, GD, and HD with Nanosize Al_2O_3. Formation of Aluminophosphonates. *J. Am. Chem. Soc.* **2001**, *123*, 1636−1644.
(8) Kanan, S. M.; Tripp, C. P. An Infrared Study of Adsorbed Organophosphonates on Silica: A Prefiltering Strategy for the Detection of Nerve Agents on Metal Oxide Sensors. *Langmuir* **2001**, *17*, 2213−2218.
(9) Katz, M. J.; Mondloch, J. E.; Totten, R. K.; Park, J. K.; Nguyen, S. T.; Farha, O. K.; Hupp, J. T. Simple and Compelling Biomimetic Metal-Organic Framework Catalyst for the Degradation of Nerve Agent Simulants. *Angew. Chem., Int. Ed.* **2014**, *53*, 497−501.
(10) Montoro, C.; Linares, F.; Quartapelle Procopio, E. Q.; Senkovska, I.; Kaskel, S.; Galli, S.; Masciocchi, N.; Barea, E.; Navarro, J. A. Capture of Nerve Agents and Mustard Gas Analogues by Hydrophobic Robust MOF-5 Type Metal-Organic Frameworks. *J. Am. Chem. Soc.* **2011**, *133*, 11888−11891.
(11) Mondloch, J. E.; Katz, M. J.; III Isley, W. C.; Ghosh, P.; Liao, P.; Bury, W.; Wagner, G. W.; Hall, M. G.; DeCoste, J. B.; Peterson, G. W.; et al. Destruction of Chemical Warfare Agents Using Metal-Organic Frameworks. *Nat. Mater.* **2015**, *14*, 512−516.
(12) Moon, S. Y.; Liu, Y.; Hupp, J. T.; Farha, O. K. Instantaneous Hydrolysis of Nerve-Agent Simulants with a Six-Connected Zirconium-Based Metal-Organic Framework. *Angew. Chem., Int. Ed.* **2015**, *54*, 6795−6799.
(13) DeCoste, J. B.; Peterson, G. W. Metal-Organic Frameworks for Air Purification of Toxic Chemicals. *Chem. Rev.* **2014**, *114*, 5695−5727.
(14) Wang, Q.; Chapleski, R. C., Jr.; Plonka, A. M.; Gordon, W. O.; Guo, W.; Nguyen-Phan, T. D.; Sharp, C. H.; Marinkovic, N. S.; Senanayake, S. D.; Morris, J. R.; Hill, C. L.; Troya, D.; Frenkel, A. I.

DOI: 10.1021/acs.jpclett.9b01002
J. Phys. Chem. Lett. 2019, 10, 2295−2299

Atomic-Level Structural Dynamics of Polyoxoniobates during DMMP Decomposition. *Sci. Rep.* **2017**, *7*, 773.
(15) Guo, W.; Lv, H.; Sullivan, K. P.; Gordon, W. O.; Balboa, A.; Wagner, G. W.; Musaev, D. G.; Bacsa, J.; Hill, C. L. Broad-Spectrum Liquid- and Gas-Phase Decontamination of Chemical Warfare Agents by One-Dimensional Heteropolyniobates. *Angew. Chem., Int. Ed.* **2016**, *55*, 7403−7407.
(16) Kinnan, M. K.; Creasy, W. R.; Fullmer, L. B.; Schreuder-Gibson, H. L.; Nyman, M. Nerve Agent Degradation with Polyoxoniobates. *Eur. J. Inorg. Chem.* **2014**, *2014*, 2361−2367.
(17) Butala, R. R.; Creasy, W. R.; Fry, R. A.; McKee, M. L.; Atwood, D. A. Lewis Acid-Assisted Detection of Nerve Agents in Water. *Chem. Commun.* **2015**, *51*, 9269−9271.
(18) Kaledin, A. L.; Driscoll, D. M.; Troya, D.; Collins-Wildman, D. L.; Hill, C. L.; Morris, J. R.; Musaev, D. G. Impact of Ambient Gases on the Mechanism of $[Cs_8Nb_6O_{19}]$-Promoted Nerve-Agent Decomposition. *Chem. Sci.* **2018**, *9*, 2147−2158.
(19) Mizrahi, D. M.; Saphier, S.; Columbus, I. Efficient Heterogeneous and Environmentally Friendly Degradation of Nerve Agents on a Tungsten-Based POM. *J. Hazard. Mater.* **2010**, *179*, 495−499.
(20) Proust, A.; Thouvenot, R.; Gouzerh, P. Functionalization of Polyoxometalates: towards Advanced Applications in Catalysis and Materials Science. *Chem. Commun.* **2008**, 1837−1852.
(21) Proust, A.; Matt, B.; Villanneau, R.; Guillemot, G.; Gouzerh, P.; Izzet, G. Functionalization and Post-Functionalization: a Step towards Polyoxometalate-Based Materials. *Chem. Soc. Rev.* **2012**, *41*, 7605−7622.
(22) Stephan, H.; Kubeil, M.; Emmerling, F.; Müller, C. E. Polyoxometalates as Versatile Enzyme Inhibitors. *Eur. J. Inorg. Chem.* **2013**, *2013*, 1585−1594.
(23) Hill, C. L. Progress and Challenges in Polyoxometalate-Based Catalysis and Catalytic Materials Chemistry. *J. Mol. Catal. A: Chem.* **2007**, *262*, 2−6.
(24) Boglio, C.; Lemiere, G.; Hasenknopf, B.; Thorimbert, S.; Lacote, E.; Malacria, M. Lanthanide Complexes of the Monovacant Dawson Polyoxotungstate $[alpha_1\text{-}P_2W_{17}O_{61}]^{10-}$ as Selective and Recoverable Lewis Acid Catalysts. *Angew. Chem., Int. Ed.* **2006**, *45*, 3324−3327.
(25) Wang, S.-S.; Yang, G.-Y. Recent Advances in Polyoxometalate-Catalyzed Reactions. *Chem. Rev.* **2015**, *115*, 4893−4962.
(26) Collins-Wildman, D. L.; Kim, M.; Sullivan, K. P.; Plonka, A. M.; Frenkel, A. I.; Musaev, D. G.; Hill, C. L. Buffer-Induced Acceleration and Inhibition in Polyoxometalate-Catalyzed Organophosphorus Ester Hydrolysis. *ACS Catal.* **2018**, *8*, 7068−7076.
(27) Wang, G.; Sharp, C.; Plonka, A. M.; Wang, Q.; Frenkel, A. I.; Guo, W.; Hill, C.; Smith, C.; Kollar, J.; Troya, D.; Morris, J. R. Mechanism and Kinetics for Reaction of the Chemical Warfare Agent Simulant, DMMP(g), with Zirconium(IV) MOFs: An Ultrahigh-Vacuum and DFT Study. *J. Phys. Chem. C* **2017**, *121*, 11261−11272.
(28) Wilmsmeyer, A. R.; Uzarski, J.; Barrie, P. J.; Morris, J. R. Interactions and Binding Energies of Dimethyl Methylphosphonate and Dimethyl Chlorophosphate with Amorphous Silica. *Langmuir* **2012**, *28*, 10962−10967.
(29) Kholdeeva, O. A.; Maksimov, G. M.; Maksimovskaya, R. I.; Vanina, M. P.; Trubitsina, T. A.; Naumov, D. Y.; Kolesov, B. A.; Antonova, N. S.; Carbó, J. J.; Poblet, J. M. Zr^{IV}-Monosubstituted Keggin-Type Dimeric Polyoxometalates: Synthesis, Characterization, Catalysis of H_2O_2-Based Oxidations, and Theoretical Study. *Inorg. Chem.* **2006**, *45*, 7224−7234.
(30) Davis, E. D.; Gordon, W. O.; Wilmsmeyer, A. R.; Troya, D.; Morris, J. R. Chemical Warfare Agent Surface Adsorption: Hydrogen Bonding of Sarin and Soman to Amorphous Silica. *J. Phys. Chem. Lett.* **2014**, *5*, 1393−1399.
(31) Wilmsmeyer, A. R.; Gordon, W. O.; Davis, E. D.; Troya, D.; Mantooth, B. A.; Lalain, T. A.; Morris, J. R. Infrared Spectra and Binding Energies of Chemical Warfare Nerve Agent Simulants on the Surface of Amorphous Silica. *J. Phys. Chem. C* **2013**, *117*, 15685−15697.
(32) Ross-Medgaarden, E. I.; Wachs, I. E. Structural Determination of Bulk and Surface Tungsten Oxides with UV-vis Diffuse Reflectance Spectroscopy and Raman Spectroscopy. *J. Phys. Chem. C* **2007**, *111*, 15089−15099.
(33) Chapleski, R. C.; Musaev, D. G.; Hill, C. L.; Troya, D. Reaction Mechanism of Nerve-Agent Hydrolysis with the $Cs_8Nb_6O_{19}$ Lindqvist Hexaniobate Catalyst. *J. Phys. Chem. C* **2016**, *120*, 16822−16830.
(34) Troya, D. Reaction Mechanism of Nerve-Agent Decomposition with Zr-Based Metal Organic Frameworks. *J. Phys. Chem. C* **2016**, *120*, 29312−29323.
(35) Plonka, A. M.; Wang, Q.; Gordon, W. O.; Balboa, A.; Troya, D.; Guo, W.; Sharp, C. H.; Senanayake, S. D.; Morris, J. R.; Hill, C. L.; Frenkel, A. I. In Situ Probes of Capture and Decomposition of Chemical Warfare Agent Simulants by Zr-Based Metal Organic Frameworks. *J. Am. Chem. Soc.* **2017**, *139*, 599−602.

DOI: 10.1021/acs.jpclett.9b01002
J. Phys. Chem. Lett. 2019, 10, 2295−2299